MOLECULAR IMAGING AND BIOLOGY

Mol Imaging Biol (2015) 17:204–213
DOI: 10.1007/s11307-014-0758-8

Published Online: 13 August 2014

World Molecular Imaging Society

RESEARCH ARTICLE

Evaluation of [^{111}In]-Labeled Zinc–Dipicolylamine Tracers for SPECT Imaging of Bacterial Infection

Douglas R. Rice,[1] Adam J. Plaunt,[1] Serhan Turkyilmaz,[1] Miles Smith,[2] Yuzhen Wang,[2] Mary Rusckowski,[2] Bradley D. Smith[1]

[1]*Department of Chemistry and Biochemistry, University of Notre Dame, Notre Dame, IN, 46556, USA*
[2]*Division of Nuclear Medicine, Department of Radiology, University of Massachusetts Medical School, Worcester, MA, 01655, USA*

Abstract

Purpose: This study prepared three structurally related zinc–dipicolylamine (ZnDPA) tracers with [^{111}In] labels and conducted biodistribution and single-photon emission computed tomography/computed tomography (SPECT/CT) imaging studies of a mouse leg infection model.

Procedures: Two monovalent tracers, ZnDPA-[^{111}In]DTPA and ZnDPA-[^{111}In]DOTA, each with a single zinc–dipicolylamine targeting unit, and a divalent tracer, Bis(ZnDPA)-[^{111}In]DTPA, with two zinc–dipicolylamine units were prepared. Organ biodistribution and SPECT and CT imaging studies were performed on living mice with a leg infection created by injection of clinically relevant Gram positive *Streptococcus pyogenes*. Fluorescent and luminescent Eu^{3+}-labeled versions of these tracers were also prepared and used to measure relative affinity for the exterior membrane surface of bacterial cells and mimics of healthy mammalian cells.

Results: All three ^{111}In-labeled radiotracers were prepared with a radiopurity of >90 %. The biodistribution studies showed that the two monovalent tracers were cleared from the body through the liver and kidney, with retained percentage injected dose for all organs of <8 % at 20 h and infected leg target to non-target ratio (T/NT) ratio of ≤3.0. Clearance of the divalent tracer from the bloodstream was slower and primarily through the liver, with a retained percentage injected dose for all organs <37 % at 20 h and T/NT ratio rising to 6.2 after 20 h. The SPECT/CT imaging indicated the same large difference in tracer pharmacokinetics and higher accumulation of the divalent tracer at the site of infection.

Conclusions: All three [^{111}In]-ZnDPA tracers selectively targeted the site of a clinically relevant mouse infection model that could not be discerned by visual external inspection of the living animal. The highest target selectivity, observed with a divalent tracer equipped with two zinc–dipicolylamine targeting units, compares quite favorably with the imaging selectivities previously reported for other nuclear tracers that target bacterial cell surfaces. The tracer pharmacokinetics depended heavily on tracer molecular structure suggesting that it may be possible to rapidly fine tune the structural properties for optimized *in vivo* imaging performance and clinical translation.

Electronic supplementary material The online version of this article (doi:10.1007/s11307-014-0758-8) contains supplementary material, which is available to authorized users.

Correspondence to: Bradley Smith; *e-mail:* smith.115@nd.edu

Key words: Zinc–dipicolylamine, Infection imaging, SPECT/CT, 111-indium, Molecular tracer
Abbreviations: DPPE-PEG$_{2000}$1,2-dipalmitoyl-sn-glycero-3-phosphoethanolamine-N-[methoxy(polyethylene glycol)-2000] (ammonium salt); POPC1-palmitoyl-2-oleoyl-sn-glycero-3-phosphatidylcholine; ZnDPAzinc–dipicolylamine

Introduction

Accurate and rapid diagnosis of bacterial infection is one of the grand challenges of modern global health care [1–3]. Early detection is crucial for patients that are immunosuppressed as a result of cancer treatment, transplantation, or an autoimmune disease because of their increased vulnerability to relatively nonvirulent microorganisms [4]. The increasing use of prosthetic devices such as artificial heart valves, gastric bands, and synthetic joints has also provided niches for bacterial colonization [5, 6]. At present, conventional microbiology-based diagnostic methods remain a clinical standard of care [7]. They typically involve examination and culture of samples taken from suspicious sites. These procedures are laborious and insensitive, and the results are often acquired too late to guide therapeutic decision making [8, 9]. It is recognized that improved non-invasive imaging technology will greatly facilitate the process of infection diagnosis [1–3].

Infection imaging methods can be divided into two major groups: indirect procedures that report the immune response to infection and molecular probe strategies that directly target the bacterial cells. The first approach focuses on host inflammatory biomarkers such as increased blood flow, vascular permeability, and the infiltration of white blood cells (WBCs). Imaging methods include single-photon emission tomography and computed tomography (SPECT/CT) detection of either [^{67}Ga]citrate or radiolabeled WBCs [9]. In addition, the positron emission tomography (PET) tracer 2-deoxy-2-[^{18}F]fluoro-D-glucose is known to accumulate in activated WBCs that are associated with infection [10]. A drawback with these immune-based methods is the inability to readily delineate sterile inflammation from bacterial colonization. Additionally, the methods are contingent on a functional immune response and thus, is not applicable for immunosuppressed patients.

Radiolabeled tracers that directly target the bacterial cells are inherently attractive for infection imaging. Various unique structural and functional bacterial targets have been investigated such as the bacterial cell wall proteins, bacteria-specific enzymes, and the DNA synthesis and translational machinery. High-affinity molecular probes have been explored including radiolabeled antibiotics, antibodies, oligomers, peptides, and bacteriophages [11–14]. Despite considerable effort, significant challenges remain for broad clinical translation of these bacteria binding systems. Recently, there has been a trend towards imaging probes that accumulate inside bacteria. These probes are fluorescent or radiolabeled biomolecules that only bacteria can absorb and metabolize, and they include derivatives of maltodextrin and uracil [15, 16]. While these bacteria accumulation strategies have shown preliminary success, more studies are required to test imaging performance with biofilms and bacteria that are metabolically dormant.

A significant structural difference between bacteria and mammalian host cells is the identity and associated electrostatic charge of the amphiphilic molecules within the cell envelope. Nearly all bacterial membranes possess a negative surface charge resulting from high fractions of the abundant anionic phospholipids and related amphiphiles. For example, the plasma membrane of Gram positive *Streptococcus pyogenes* (the bacterial system employed in this present study) contains significant fractions of the anionic phospholipids phosphatidylglycerol (~20 %) and cardiolipin (~5 %) [17]. We have discovered that synthetic zinc–dipicolylamine (ZnDPA) coordination complexes have high affinity for anionic cell membranes, and they can selectively target bacterial cells over the zwitterionic membrane surfaces of healthy mammalian cells [18–24]. Fluorescent ZnDPA probes have been shown to stain Gram positive and Gram negative bacteria and near-infrared fluorescent versions are effective for *in vivo* imaging of infection in rodents [19, 22]. The clinical utility of optical imaging probes is limited and there is a need to synthesize and evaluate radiolabeled ZnDPA tracers for infection imaging. To date, a preliminary SPECT imaging study of a nanoparticle construct, comprised of streptavidin protein decorated with biotinylated ZnDPA and chelated ^{111}In, has been shown to selectively target infection over sterile inflammation in a mouse model [25]. Small molecule versions of ZnDPA tracers with ^{99m}Tc and ^{18}F labels have been prepared but not yet evaluated for infection imaging [26–28]. This present report describes a mouse biodistribution and preliminary SPECT imaging study that evaluates three, low molecular weight ZnDPA tracers labeled with ^{111}In. We find that all three tracers selectively accumulate at the site of a clinically relevant *S. pyogenes* leg infection. The highest target selectivity, observed with a divalent tracer equipped with two zinc–dipicolylamine targeting units, compares quite favorably with the *in vivo* imaging selectivities reported for other nuclear tracers that target bacterial cell surfaces.

Materials and Methods

Radiolabeling of ZnDPA–Chelator Conjugates

Synthesis and characterization of the three precursor DPA-chelator conjugates is described in the Electronic Supplementary Material. In each case, the Zn^{2+} complex was formed by combining methanol solutions of the precursor DPA-chelator conjugate and zinc nitrate in a 2.2:1 M ratio and shaking the solution for 45 min at room temperature. The solvent was evaporated to give the desired ZnDPA–chelator conjugate with no further purification. Radiolabeling was achieved by mixing an appropriate aliquot of $^{111}InCl_3$ from a stock solution of 2 mCi/10 µl in 0.05-M HCl (purchased from PerkinElmer) and an equal volume of sodium acetate (0.5 M; pH 5.7) and incubating at 25 °C for 30 min. The solution was then mixed with one of the three ZnDPA–chelator conjugates in sodium acetate (0.1 M; pH 6.1) and incubated for 1-h (DTPA conjugates) or 3 h (DOTA conjugate) at 50 °C. The specific activity of each tracer for the biodistribution and SPECT imaging experiments was kept close to 3 µCi/µg.

The radiochemical purity was determined using reverse-phase HPLC system equipped with a 515 pump, an in-line dual UV/radioactivity detector under the control of Millennium 32 software (Waters, Milford, MA). A Jupiter C18 column (90 Å pore size, 250 mm×4.6 mm) was employed with a buffered mobile phase system consisting of mobile phase A (99.9 % water, 0.1 % TFA, pH 6.7) and mobile phase B (99.9 % acetonitrile, 0.1 % TFA) at a flow rate of 1.0 ml/min at room temperature. A baseline of 5 min at 90 % mobile phase A and 10 % mobile phase B was followed by a linear gradient to 10 % mobile phase A and 90 % mobile phase B in 30 min. The retention times of the ^{111}In-labeled tracers matched the retention times of cold versions. The level of radioactivity in the HPLC elute was monitored by the in-line radioactivity detector and the percent ^{111}In for each peak was calculated from the integrated area.

Fluorescence Microscopy of Streptococcus Pyogenes

S. Pyogenes (ATCC 19615) was cultured in Luria broth (LB) containing no antibiotic after transfer from a preserved sample stored at 4 °C. Cells were allowed to grow overnight by incubating at 37 °C. Samples of 10^7 colony forming units (CFU) were centrifuged at 10,000 rpm for 5 min. Growth media was removed, and the cells resuspended in 10-mM HEPES buffer (137-mM NaCl, 3.2-mM KCl, pH 7.4). Cells were then treated with 50 nmol of PSVue643 (purchased from Molecular Targeting Technologies Inc.) and the mixture was incubated in the dark for 15 min at room temperature. After centrifugation at 10,000 rpm for 5 min, the media was discarded and the pellet resuspended in 10-mM HEPES buffer with vortexing. The stained cells were rinsed with HEPES buffer by repeating the centrifugation/resuspension cycle. Fluorescence microscopy was conducted on a Nikon Eclipse TE-2000 U epifluorescence microscope equipped with Cy5 (exciter: HQ620/60X, dichroic: 660LP, emitter: HQ700/75 m) filter. Images were acquired using Nikon RL software (v 6.2 Molecular Devices, Sunnyvale, CA) and a Photometrics 512 B black and white digital camera (×100) at 150-ms acquisition time.

Membrane Association Studies Using Eu^{3+}-labeled ZnDPA Tracers

The preparation of vesicles composed of POPC:Cholesterol:2,3-Naphthalimide:DPPE-PEG_{2000} in the molar ratio of 72:10:10:8 and synthesis of photoactive Eu-labeled ZnDPA tracers (Fig. 1) is described in the Electronic Supplementary Material. The titration experiment added aliquots of Eu-labeled ZnDPA tracer to separate solutions of vesicles (100-µM final concentration) in HEPES buffer (10-mM HEPES, 137-mM NaCl, 3.2-mM KCl, pH 7.4) at 25 °C. After waiting 60 s for equilibration to occur, energy transfer from

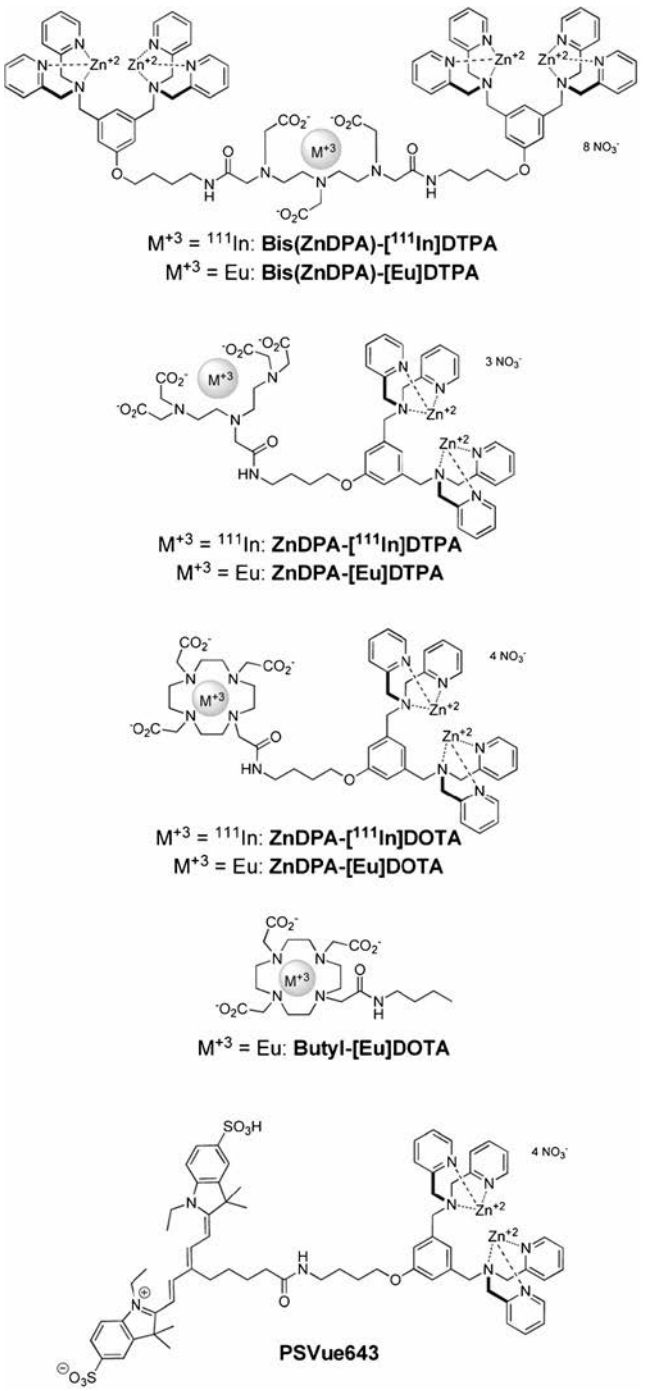

Fig. 1 Chemical structures.

the 2,3-naphthalimide within the vesicle membrane to Eu-labeled ZnDPA tracer associated with the vesicle surface was measured (λ_{ex}=332 nm, λ_{em}=570–630 nm) using a fluorescence spectrometer equipped with a 50-nm band pass filtered centered at 600 nm. Plots of Eu emission intensity at 592 nm were generated as a function of Eu-labeled ZnDPA tracer concentration.

Serum Protein Association Studies Using Eu-labeled ZnDPA Tracers

Qualitative equilibrium dialysis assays were used to measure tracer affinity to serum albumin. Experiments employed an equilibrium dialysis cell consisting of two compartments, "source" and "receiver," separated by a 10,000 molecular weight cutoff membrane that was impermeable to albumin proteins. Briefly, either TES buffer (10-mM TES, 145-mM NaCl, pH 7.4) or bovine serum albumin (80 %) was added to the receiver compartment (750 µl) of the equilibrium dialysis apparatus while a Eu-labeled ZnDPA tracer (20 µM) in TES buffer (10-mM TES, 145-mM NaCl, pH 7.4) was added to the source compartment (750 µl). The system was allowed to equilibrate by shaking at 180 rpm and 37 °C for 24 h. The amount of ZnDPA tracer in each compartment was determined using a colorimetric indicator, NO_2-PAPS, as previously described [29]. Control experiments confirmed that an unbiased dialysis equilibrium occurred in the absence of serum albumin.

Radiotracer Biodistribution in Mouse Leg Infection Model

All animal studies were performed with the approval of the UMMS Institutional Animal Care and Use Committee. The following biodistribution experiment was conducted with each of the three radiolabeled ZnDPA tracers. Two cohorts of healthy CD-1 nude mice (each cohort n=4 males 20–25 g, Charles River) were given a bolus injection of *S. Pyogenes* (5×10^8 CFU in 100 µl of LB growth media, determined by plating of serial dilutions on agar plates) injected into the target (T) muscles that overlay the tibia bone in the right posterior leg. The same volume of saline was injected into the contralateral leg which was treated as the non-target site (NT). The mice were allowed to recover for 3 h, before dosing *via* the tail vein with radiolabeled ZnDPA tracer (~150 µl, 20 µCi) in saline. After 1 h, one cohort was anesthetized and sacrificed, and the second cohort was sacrificed after 20 h. The organs were excised, weighed, and radioactivity counted using a NaI (T1) automatic gamma counter against a standard of the injectate. The percent injected dose per gram of tissue (%ID/g) was calculated and the target to non-target ratio (T/NT) was determined using the values of percent injected dose per gram of tissue for the infected and normal legs.

SPECT/CT Imaging of Mouse Leg Infection Model

The following imaging experiments were conducted with each of the three radiolabeled ZnDPA tracers using a NanoSPECT/CT (Bioscan, Washington, DC) small animal camera. A bolus of *S. Pyogenes* (5×10^8 CFU) in 100 µl of LB growth media was injected into the muscles that overlay the right tibia bone of a cohort of healthy CD-1 mice (n=2). As a control, the same volume of saline was injected into the contralateral leg. The mice were allowed to recover for 3 h before intravenous injection with radiolabeled ZnDPA tracer (~150 µl, 450 µCi) in saline *via* the tail vein. Each mouse was imaged at approximately 1, 4, and 20 h after tracer injection. In each case, the mice were anesthetized with 1–2 % isoflurane in oxygen and whole body scans were acquired. A CT acquisition, requiring about 4 min, was performed before each SPECT acquisition, at standard frame resolution, 180 projections, 45-kVp tube voltage and 500 ms of exposure time. The SPECT image was acquired with a 256×256 frame size and 24 projections. The time per projection was adjusted to collect approximately 50,000 counts/detector for each projection. For initial scans, this required 50 s/projection (total scan time of 30 min) and was increased to a maximum of 110 s/projection (total scan time of 60 min). The SPECT and CT reconstructions and volume-of-interest analysis of the SPECT acquisitions were performed using InVivoScope 1.43 software (Bioscan, Washington, DC).

Statistical Analysis

The Student's t test was used for significance determination where indicated.

Results

Tracer Synthesis

Shown in Fig. 1 are the three sets of ZnDPA tracers that were prepared and studied. The cold Eu-labeled structures were prepared for two reasons: (a) to confirm that the DOTA and DTPA chelators within the precursor DPA conjugates were vacant and available for heavy metal chelation and (b) to enable the membrane association assay described below. The three ^{111}In-labeled ZnDPA tracers were prepared by sequentially converting the precursor DPA-chelator conjugates into Zn^{2+} complexes and then into $^{111}In^{3+}$ chelates. A previous titration study of a related DPA-chelator conjugate proved that the Zn^{2+} complexation is specific for the DPA units and the heavy metal cations occupy the attached DTPA or DOTA chelator [30]. Figure 2 shows reverse-phase HPLC radiochromatograms of the three ^{111}In labeled ZnDPA tracers. The retention time and radiopurity for each tracer

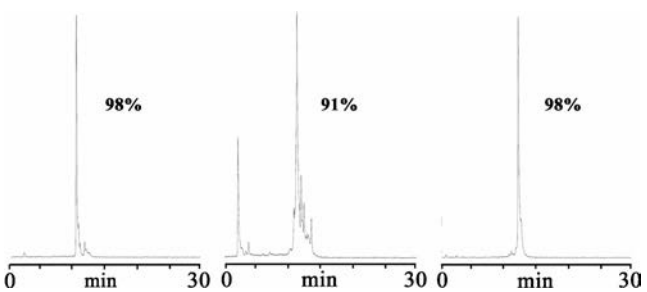

Fig. 2 HPLC radiochromatograms and radiopurities of Bis(ZnDPA)-[^{111}In]DTPA (*left*), ZnDPA-[^{111}In]DOTA (*middle*), and ZnDPA-[^{111}In]DTPA (*right*). The retention times are 12.3, 13.2, and 13.4 min, respectively. The uncomplexed ^{111}In eluted at ~3 min.

was 13.2 min and 91 % for ZnDPA-[^{111}In]DOTA, 12.3 min and 98 % for ZnDPA-[^{111}In]DTPA, 13.4 min and 98 % for Bis(ZnDPA)-[^{111}In]DTPA. The samples were judged pure enough for immediate dosing without further purification. Samples that were incubated in serum solution for 24 h showed no HPLC evidence of tracer decomposition, in agreement with previous observations that this class of ZnDPA conjugates is quite stable in biological media [26, 22, 31].

It is important to note that ZnDPA-[^{111}In]DTPA and ZnDPA-[^{111}In]DOTA, each contain only a single zinc–dipicolylamine targeting unit and are considered to be monovalent tracers while Bis(ZnDPA)-[^{111}In]DTPA contains two zinc–dipicolylamine targeting units and is considered a divalent tracer.

Fluorescence Microscopy of Streptococcus Pyogenes

Targeting of a low molecular weight, ZnDPA tracer to *S. Pyogenes* cells was verified using fluorescence microscopy. Figure 3 shows images of intensely stained *S. Pyogenes* cells after treatment with PSVue643, a commercially available deep-red, fluorescent ZnDPA tracer [31].

Membrane and Serum Association Studies Using Eu-labeled Tracers

The propensity for lipophilic association of the ZnDPA tracers with biological surfaces was assessed in two ways. One was a membrane association assay using vesicle membranes composed of POPC:Cholesterol:2,3-Naphthalimide:DPPE-PEG_{2000} in the molar ratio of 72:10:10:8. The large fraction of zwitterionic POPC and cholesterol mimics the plasma membrane composition of healthy mammalian cells. The small fraction of DPPE-PEG_{2000} was included to inhibit any vesicle crosslinking, a phenomena that was observed when anionic vesicles (mimics of bacterial cell membranes) were treated with the divalent tracer. The assay monitored energy transfer from membrane-bound photosensitizer (2,3-naphthalimide) to any Eu-labeled ZnDPA tracer that associated with the vesicle surface (Scheme S1) [32]. The titration plots in Fig. 4 reflect the relative membrane affinity of the four Eu-labeled complexes in Fig. 1. The data shows that the order of membrane association is butyl-[Eu]DOTA>ZnDPA-[Eu]DOTA>ZnDPA-[Eu]DTPA~Bis(ZnDPA)-[Eu]DTPA. This trend is consistent with literature knowledge that lanthanide DOTA complexes are more lipophilic than lanthanide DTPA complexes [33, 34]. Furthermore, attachment of a second ZnDPA unit increases the molecular hydrophilicity.

The relative affinity of the three Eu-labeled tracers for serum proteins was determined using an equilibrium dialysis assay. The results are presented in Fig. 5 as a dialysis ratio, with a value greater than 1 reflecting sequestration of the tracer by the serum albumin in the receiver compartment of the dialysis apparatus. The data shows that there is modest serum protein affinity for ZnDPA-[Eu]DTPA but very little for ZnDPA-[Eu]DOTA and Bis(ZnDPA)-[Eu]DTPA. The higher albumin affinity for ZnDPA-[Eu]DTPA compared to the more lipophilic ZnDPA-[Eu]DOTA is counterintuitive but the structural reason was not pursued because ^{111}In labeled versions of these monovalent tracers exhibited very similar mouse biodistribution profiles (see below). Apparently, the difference in albumin affinity does not translate into altered pharmacokinetics.

^{111}In Tracer Biodistribution in Mouse Leg Infection Model

The biodistribution of each radiolabeled ZnDPA tracer in the mouse infection model was determined at 1 and 20 h after tracer dosage. For each tracer, two separate cohorts of healthy CD-1 mice (n=4) were inoculated with *S. Pyogenes* (5×10^8 CFU) in the target posterior leg (T) and saline in the contralateral normal leg (NT). This bacterial burden did not produce externally visible evidence of swelling or redness—the mice looked and behaved as if uninfected. Three hours later, both cohorts were dosed intravenously

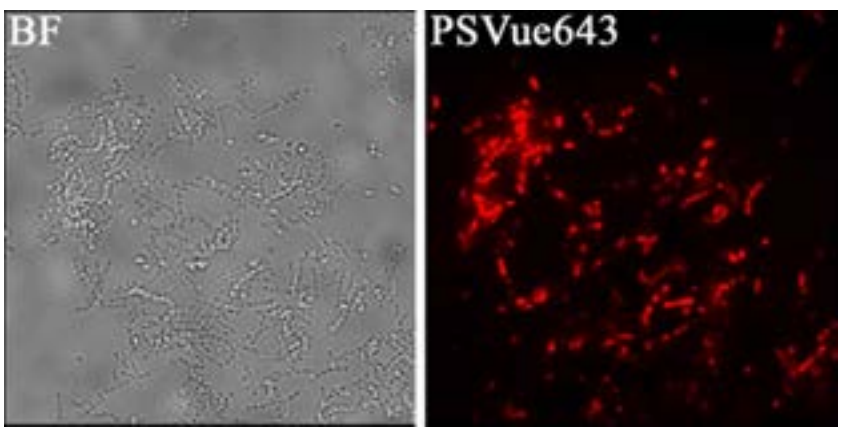

Fig. 3 Fluorescence micrographs (*brightfield* and *deep-red fluorescence*) of *S. Pyogenes* stained with PSVue643.

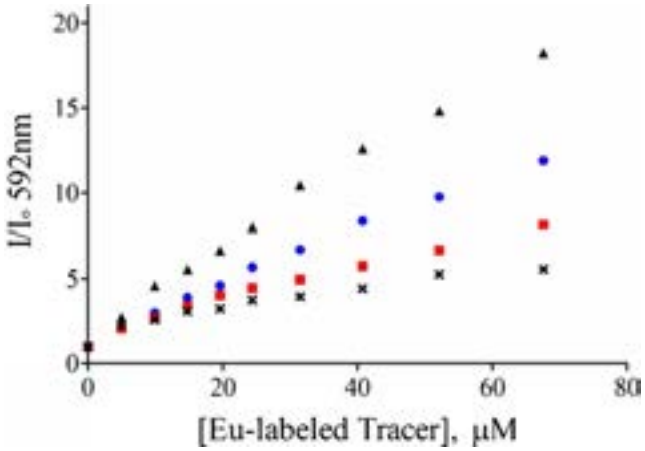

Fig. 4 Vesicle membrane association assay. Change in Eu emissiom at 592 nm due to addition of Bis(ZnDPA)-[Eu]DTPA (*black cross*), ZnDPA-[Eu]DTPA (*red square*), ZnDPA-[Eu]DOTA (*blue circle*), and Butyl-[Eu]DOTA (*black triangle*) to separate dispersions of vesicles composed of POPC:Cholesterol:2,3-Naphthalimide:DPPE-PEG$_{2000}$ (molar ratio of 72:10:10:8) in HEPES buffer (10-mM HEPES, 137-mM NaCl, 3.2-mM KCl, pH 7.4) at 25 °C.

with radiolabeled ZnDPA tracer. One cohort was sacrificed after 1 h and the second cohort after 20 h. Table 1 presents the biodistribution results as percent injected dose per gram (%ID/g) for each organ and leg infection target to non-target ratio (T/NT). The tracers exhibit quite different biodistribution profiles. The monovalent tracers (ZnDPA-[^{111}In]DTPA and ZnDPA-[^{111}In]DOTA) were excreted at about the same rate; the retained percentage injected dose by all organs was <50 % at 1 h and <8 % at 20 h. The organs retaining the highest %ID/g at 1 h were the liver, kidney, intestines, and blood. The T/NT rose to 3.0 and 2.4 at 20 h for ZnDPA-[^{111}In]DTPA and ZnDPA-[^{111}In]DOTA, respectively. In contrast, clearance of the divalent tracer, Bis(ZnDPA)-[^{111}In]DTPA, was slower and there was higher accumulation at the site of infection. The retained percentage injected dose by all organs was 62 % at 1 h and 37 % at 20 h, with the vast majority of the retained dose in the liver. The T/NT was 2.8 at 1 h and 6.2 at 20 h.

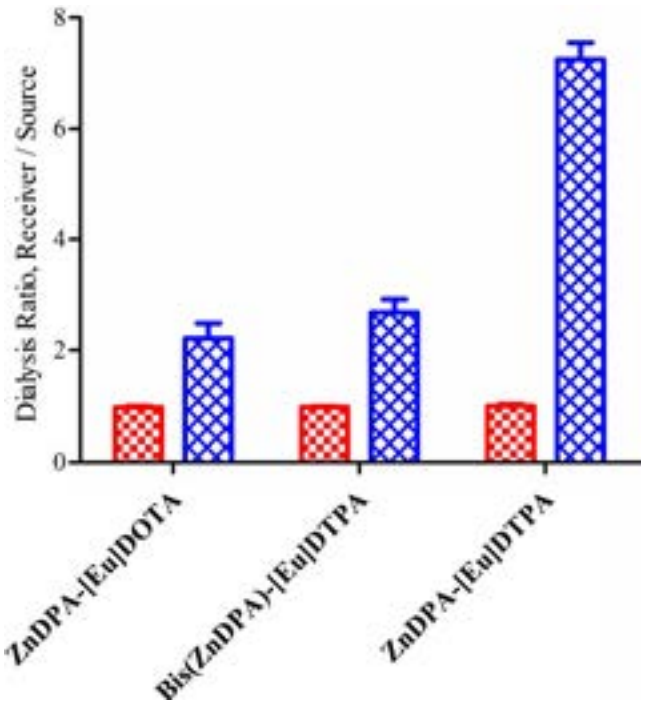

Fig. 5 Equilibrium dialysis ratio reflecting affinity of three Eu-labeled tracers towards either TES buffer (*red*) or bovine serum albumin (*blue*).

SPECT/CT Imaging of Mouse Leg Infection Model

The SPECT/CT imaging studies employed a 22-fold higher tracer dose, but the same general tracer biodistribution trends were observed. Analysis of the SPECT data enabled determination of the percent injected dose remaining in the body of the infected mice at three different time points after tracer injection (Table 2). After the last time point of 20 h, there was 1, 6, and 55 % of injected dose remaining with the tracers, ZnDPA-[^{111}In]DTPA, ZnDPA-[^{111}In]DOTA, and Bis(ZnDPA)-[^{111}In]DTPA, respectively. Figure 6 shows representative whole body SPECT/CT images of an infected mouse after dosing with the divalent tracer Bis(ZnDPA)-[^{111}In]DTPA. The areas of highest tracer accumulation were the liver and intestines, with significant and selective targeting of the infected leg. At 20 h, there was sufficient image resolution at the site of infection to clearly delineate tracer accumulation in the edema surrounding the infected muscle, an observation that is consistent with abscess formation. A volume-of-interest comparison of the infected leg (T) compared to the normal leg (NT) showed that the T/NT ratio peaked at 1 and 4 h, in the cases of ZnDPA-[^{111}In]DTPA and ZnDPA-[^{111}In]DOTA, respectively (Table 2). The highest T/NT ratio (4.0) observed by SPECT imaging was obtained using Bis(ZnDPA)-[^{111}In]DTPA and that was measured at 20 h after tracer dosing. Montages of infected mice, dosed with each of the three tracers, are provided in the Electronic Supplementary Material (Fig. S2).

Discussion

Our previous studies of fluorescent ZnDPA probes has shown that they exhibit highly selective targeting of Gram positive and Gram negative bacteria in the presence of healthy mammalian cells [18–24]. Furthermore, animal imaging studies have shown that ZnDPA probes accumulate in sites of bacterial infection and not in sites of sterile inflammation [24, 25]. Histological analyses of the infected tissue indicate high levels of probe localization with the bacterial cells [22]. Since ZnDPA probes also target the anionic surfaces of dead/dying mammalian cells, it is possible that probe accumulation in sites of chronic infection

Table 1. Biodistribution of radiolabeled tracers in organs from mice with *S. Pyogenes* leg infection

	ZnDPA-[^{111}In]DTPA		ZnDPA-[^{111}In]DOTA		Bis(ZnDPA)-[^{111}In]DTPA	
Organ	1 h	20 h	1 h	20 h	1 h	20 h
Liver	3.41 (0.34)	3.30 (0.50)	4.02 (0.57)	0.93 (0.16)	16.88 (6.71)	18.11 (1.83)
Heart	1.67 (0.15)	0.27 (0.10)	1.67 (0.28)	0.09 (0.02)	6.35 (0.52)	0.52 (0.13)
Kidney	4.27 (0.66)	1.06 (0.24)	5.19 (2.18)	0.51 (0.04)	6.54 (1.09)	2.75 (0.60)
Lung	1.01 (0.56)	0.13 (0.03)	1.61 (0.93)	0.08 (0.01)	5.15 (4.91)	0.53 (0.14)
Spleen	0.83 (0.21)	0.39 (0.10)	0.93 (0.36)	0.13 (0.03)	3.08 (3.21)	1.64 (0.71)
Stomach	0.93 (0.30)	0.09 (0.06)	1.83 (1.06)	0.07 (0.05)	1.88 (0.81)	0.42 (0.52)
Intestines	4.92 (1.88)	0.10 (0.03)	10.40 (2.34)	0.08 (0.01)	3.22 (0.97)	0.56 (0.29)
Normal leg	0.69 (0.06)	0.04 (0.01)	1.30 (0.34)	0.05 (0.01)	1.11 (0.30)	0.18 (0.06)
Infected leg	1.49 (0.32)	0.12 (0.01)	1.61 (0.23)	0.12 (0.02)	3.16 (1.26)	1.11 (0.43)
Blood	3.91 (0.84)	0.10 (0.05)	4.70 (0.99)	0.03 (0.01)	17.68 (1.95)	0.44 (0.19)
T/NT[a]	2.1 (0.053)	3.0 (0.002)	1.2 (0.479)	2.4 (0.023)	2.8 (0.164)	6.2 (0.025)

Values are mean %ID/g with standard deviation from the mean (n=4)
[a]Ratio of %ID/g for infected leg (T) to normal leg (NT) with P value

may also be due to ZnDPA association with dead/dying inflammatory cells or dead/dying host cells that have become infected with bacteria. In other words, the ZnDPA probes could be behaving as a mimic of the cell death probe annexin V [35]. But this is unlikely to be a major targeting process in this present study, since an acute infection model was employed with no visible evidence of host tissue necrosis. *S. pyogenes* is a clinically relevant bacterial infection that is associated with invasive disease having a high mortality. The infection burden of 10^8 CFU used in our experiments is comparable to the bacterial levels found in clinical Gram positive infections [36–38]. Previous imaging studies have demonstrated that ZnDPA probes can selectively target *S. pyogenes* over host tissue in a mouse infection model [25]. Confirmation of direct bacterial cell targeting ability was gained by conducting fluorescence microscopy experiments that imaged cell staining by PSVue643, a deep-red fluorescent ZnDPA probe (Fig. 3). The three tracer designs in Fig. 1 are amide bond conjugates of ZnDPA targeting groups linked to a chelator that is occupied with a reporting heavy metal cation. Cold Eu-labeled versions were prepared and used to measure non-selective association with serum proteins and a vesicle mimic of the mammalian cell plasma membrane [32]. Both sets of assays concluded that the divalent tracer, Bis(ZnDPA)-[Eu]DTPA, is relatively hydrophilic and does not have strong affinity for lipophilic binding sites within proteins or relatively uncharged bilayer membranes.

The three ^{111}In-labeled tracers in Fig. 1 were prepared in >90 % radiochemical purity. ^{111}In was employed as the reporter isotope for two reasons: synthetic convenience, and its long half life (~67 h) which enables longitudinal studies. The two monovalent tracers, ZnDPA-[^{111}In]DTPA and ZnDPA-[^{111}In]DOTA, allowed a comparative assessment of the effect of chelator structure (DTPA vs DOTA) on biodistribution [33, 34]. The membrane association assay (Fig. 4) indicated that the DOTA analog was slightly more lipophilic, however, the biodistribution data showed that both monovalent tracers cleared equally rapidly through the liver and kidney and the SPECT imaging showed that the T/NT ratios (≤3.0) peaked within a few hours. These results reflect the relatively modest affinity of the monovalent tracers for the target bacteria cells. In comparison, multivalent ZnDPA probes such as the divalent Bis(ZnDPA)-[^{111}In]DTPA are known to exhibit enhanced bacterial affinity and a propensity to induce bacteria cell agglutination [39]. Clearance of the divalent tracer from the bloodstream was comparatively slow and primarily through the liver with high accumulation at the infection site. This clearance profile differs substantially from the related ^{111}In-DOTA-biotin/avidin/biotin-ZnDPA nanoparticle system described by Liu et al. which accumulated strongest in the kidneys and bladder with minimal accumulation at the liver [25]. The T/NT ratio of the divalent probe rose to a value of 6.2 at 20 h. This compares favorably to the reported performance of other bacteria-targeted probes in the literature. For

Table 2. Ratio of the infected leg (T) to normal leg (NT), and percent of injected dose remaining in the whole body of mice with *S. Pyogenes* leg infection, determined from SPECT imaging

Time (hours)	ZnDPA-[^{111}In]DTPA		ZnDPA-[^{111}In]DOTA		Bis(ZnDPA)-[^{111}In]DTPA	
	% Dose remaining	T/NT	% Dose remaining	T/NTT	% Dose remaining	T/NT
1	39	2.0	45	1.6	87	3.0
4	22	1.9	25	3.0	80	2.4
20	1	1.3	6	1.6	55	4.0

Values are mean of n=2

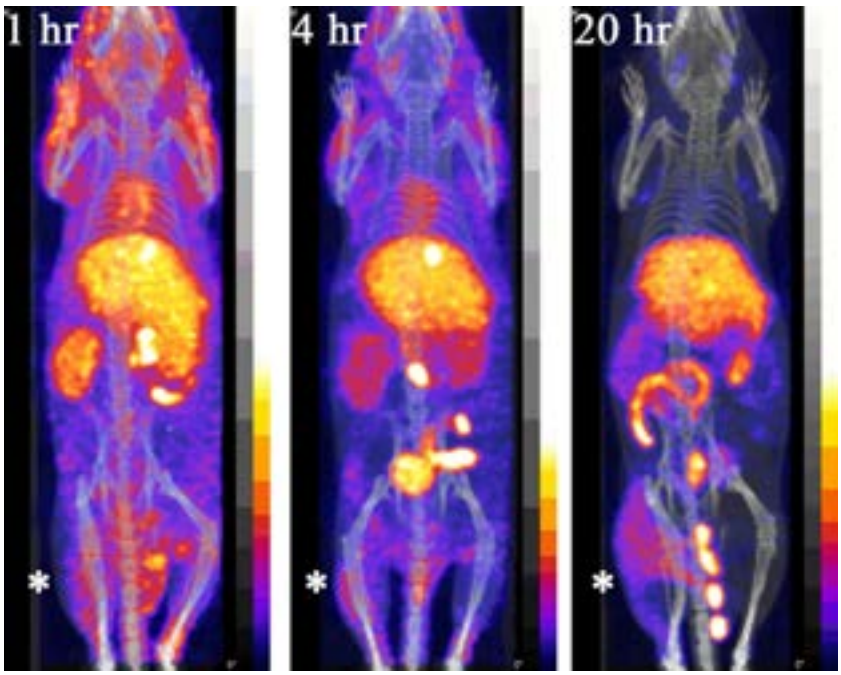

Fig. 6 Representative SPECT/CT whole body images of a mouse, with *S. Pyogenes* leg infection, at time points after dosing with Bis(ZnDPA)-[^{111}In]DTPA. The *asterisk* indicates the infected leg ($n=2$). The *gray scale bars* refer to the CT images and are proportional to Hounsfield units, and the *color scale bars* refer to the SPECT images and are proportional to percent count intensities.

example, the radiolabeled antibiotic 99mTc-pheophorbide-a produced a T/NT ratio of 5.6 for infection in rats [40]. Technetium-99m-labeled ubiquicidin peptide (99mTc-UBI), a cationic human antimicrobial peptide fragment, realized T/NT ratios between 2 and 3.5 in an infected mouse leg model [41–43], and the radiolabeled antibiotic 99mTc-vancomycin produced a T/NT ratio of five in infected rats [44].

The superior bacteria targeting of the divalent tracer was expected based on our earlier work with fluorescent versions and the fact that the SPECT/CT imaging could identify a site of infection that was not obvious by visual external inspection of the living animal is a notable achievement. Furthermore, the resolution of the SPECT/CT image at 20-h post divalent tracer injection was sufficient to reveal the beginning of abscess formation. With immune-competent mice, abscesses are formed as a defensive mechanism to prevent the spread of bacteria to other parts of the body. Abscess visualization has been previously observed with a number of magnetic resonance contrast agents [45–47].

The membrane and serum protein association experiments with stable Bis(ZnDPA)-[Eu]DTPA tracer showed that it is more hydrophilic than the two monovalent versions. Thus, the high level of Bis(ZnDPA)-[^{111}In]DTPA accumulation in the liver and intestines is not because of enhanced association with blood proteins. Transchelation of the radiolabel by metal scavengers in the bloodstream is also very unlikely since Hnatowich et al. showed that the ^{111}In transfer rate from DTPA to transferrin is ~5 %/day [48]. It appears that the slow body clearance and high liver uptake of the divalent tracer is related to its propensity to form cross-linked aggregates with anionic particles and molecules such as bacterial and inflammation cells and the phosphorylated molecular components. The liver is a critical defense component against bacteremia and is known to rapidly sequester large amounts of systemic bacteria [49, 50]. Thus, future imaging studies with next-generation ZnDPA tracers should investigate modified molecular structures that maintain the high affinity for bacterial cells but do not exhibit crosslinking effects. Our recent development of high throughput synthesis and screening methods for next-generation ZnDPA membrane recognition units is expected to greatly facilitate this tracer discovery process [29]. The fact that relatively minor structural changes in tracer structure can produce large differences in pharmacokinetic properties suggests that it may be possible to rapidly optimize *in vivo* imaging performance.

Conclusions

The synthesis of three radiolabeled [^{111}In]ZnDPA was achieved with radiopurity >90 %. Biodistribution and SPECT/CT imaging shows that the two monovalent tracers clear relatively rapidly from the mouse body through the liver and kidney with modest selective targeting of the site on leg infection. The divalent tracer exhibited significantly higher targeting to an infection site that otherwise could not be discerned by visual external inspection of the living animal. The high selectivity of the divalent tracer compares quite favorably with the selectivities previously reported for

other nuclear imaging tracers that target bacterial cell surfaces.

Acknowledgments. We are grateful for funding support from NIH grants RO1GM059078 (B. D. S.) and T32GM075762 (D. R. R.), and the Notre Dame Integrated Imaging Facility (NDIIF).

Conflict of Interest. The authors declare no conflicts of interest.

References

1. Goldsmith SJ, Vallabhajosula S (2009) Clinically proven radiopharmaceuticals for infection imaging: mechanisms and applications. Semin Nuc Med 39:2–10
2. Bunschoten A, Welling MM, Tennaat MF et al (2013) Development and prospects of dedicated tracers for the molecular imaging of bacterial infections. Bioconjug Chem 24:1971–1989
3. Sasser TA, Van Avermaete AE, White A et al (2013) Bacterial infection probes and imaging strategies in clinical nuclear medicine and preclinical molecular imaging. Curr Top Med Chem 13:479–487
4. Rubin RH, Fischman AJ (1996) Radionuclide imaging of infection in the immunocompromised host. Clin Infect Dis 22:414–423
5. Gemmel F, Van den Wyngaert H, Love C et al (2012) Prosthetic joint infections: radionuclide state-of-the-art imaging. Eur J Nuc Med Mol I 39:892–909
6. Zhou D-B, Better N (2004) Radionuclide imaging for the detection of cardiac infection. Heart Lung Circ 13:10–12
7. Craig JC, Williams GJ, Jones M et al (2010) The accuracy of clinical symptoms and signs for the diagnosis of serious bacterial infection in young febrile children: prospective cohort study of 15 781 febrile illnesses. Brit Med J 340:c1594
8. Wilcox MH (2012) Overcoming barriers to effective recognition and diagnosis of Clostridium difficile infection. Clin Microbiol Infect 18:13–20
9. Signore A, Glaudemans A (2011) The molecular imaging approach to image infections and inflammation by nuclear medicine techniques. Ann Nucl Med 25:681–700
10. Lankinen P, Lehtimaki K, Hakanen AJ et al (2012) A comparative 18F-FDG PET/CT imaging of experimental *Staphylococcus aureus osteomyelitis* and *Staphylococcus epidermidis* foreign-body-associated infection in the rabbit tibia. EJNMMI Res 2:41
11. Lambrecht FY (2011) Evaluation of Tc-99 m-labeled antibiotics for infection detection. Ann Nucl Med 25:1–6
12. Embleton ML, Nair SP, Cookson BD et al (2002) Selective lethal photosensitization of methicillin-resistant *Staphylococcus aureus* using an IgG-tin(IV) chlorin e6 conjugate. J Antimicrob Chemother 50:857–864
13. Chen L, Wang Y, Cheng D et al (2013) ^{99m}Tc-MORF oligomers specific for bacterial ribosomal RNA as potential specific infection imaging agents. Bioorg Med Chem 21:6523–6530
14. Rusckowski M, Gupta S, Liu GZ et al (2008) Investigation of four Tc-99 m-labeled bacteriophages for infection-specific imaging. Nucl Med Biol 35:433–440
15. Ning XH, Lee S, Wang ZR et al (2011) Maltodextrin-based imaging probes detect bacteria in vivo with high sensitivity and specificity. Nat Mater 10:602–607
16. Bettegowda C, Foss CA, Cheong I et al (2005) Imaging bacterial infections with radiolabeled 1-(2'-deoxy-2'-fluoro-beta-D-arabinofuranosyl)-5-iodouracil. Proc Natl Acad Sci U S A 102:1145–1150
17. Rosch JW, Hsu FF, Caparon MG (2007) Anionic lipids enriched at the ExPortal of *Streptococcus pyogenes*. J Bacteriol 189:801–806
18. Euliss LE (2006) Selective recognition of bacterial membranes achieved by zinc(II) coordination complexes. MRS Bull 31:368–368
19. Leevy WM, Gammon ST, Jiang H et al (2006) Optical imaging of bacterial infection in living mice using a fluorescent near-infrared molecular probe. J Am Chem Soc 128:16476–16477
20. Johnson JR, Fu N, Arunkumar E et al (2007) Squaraine rotaxanes: superior substitutes for Cy-5 in molecular probes for near-infrared fluorescence cell imaging. Angew Chem Int Ed 46:5528–5531
21. DiVittorio KM, Leevy WM, O'Neil EJ et al (2008) Zinc(II) coordination complexes as membrane-active fluorescent probes and antibiotics. ChemBioChem 9:286–293
22. Leevy WM, Gammon ST, Johnson JR et al (2008) Noninvasive optical imaging of *Staphylococcus aureus* bacterial infection in living mice using a bis-dipicolylamine-zinc(II) affinity group conjugated to a near-infrared fluorophore. Bioconjug Chem 19:686–692
23. Leevy WM, Lambert TN, Johnson JR et al (2008) Quantum dot probes for bacteria distinguish *Escherichia coli* mutants and permit in vivo imaging. Chem Commun 20:2331–2333
24. White AG, Fu N, Leevy WM et al (2010) Optical imaging of bacterial infection in living mice using deep-red fluorescent squaraine rotaxane probes. Bioconjug Chem 21:1297–1304
25. Liu XR, Cheng DF, Gray BD et al (2012) Radiolabeled Zn-DPA as a potential infection imaging agent. Nucl Med Biol 39:709–714
26. Wyffels L, Gray BD, Barber C et al (2011) Synthesis and preliminary evaluation of radiolabeled bis(zinc(II)-dipicolylamine) coordination complexes as cell death imaging agents. Bioorg Med Chem 19:3425–3433
27. Wang HL, Tang XL, Tang GH et al (2013) Noninvasive positron emission tomography imaging of cell death using a novel small-molecule probe, F-18 labeled bis(zinc(II)-dipicolylamine) complex. Apoptosis 18:1017–1027
28. Li J, Gray BD, Pak KY et al (2012) Radiolabeling and optimizing of zinc(II) dipicolylamine (DPA) with three 18 F-prosthetic groups (18 F-NFP, 18 F-SFB, and18F-FET) as potential infectious imaging agents. J Label Compd Radiopharm 55:149–154
29. Plaunt AJ, Harmatys KM, Wolter WR et al (2014) Library synthesis, screening, and discovery of modified zinc(II)-bis(dipicolylamine) probe for enhanced molecular imaging of cell death. Bioconjug Chem. doi:10.1021/bc500003x
30. Matosziuk LM, Harney AS, MacRenaris KW, et al. (2012) Synthesis, characterization, and in vitro testing of a bacteria-targeted MR contrast agent. Eur J Inorg Chem 2099-2107
31. White AG, Gray BD, Pak KY et al (2012) Deep-red fluorescent imaging probe for bacteria. Bioorg Med Chem Lett 22:2833–2836
32. Surman AJ, Kenny GD, Kumar DK et al (2011) Targeting of anionic membrane species by lanthanide(III) complexes: towards improved MRI contrast agents for apoptosis. Chem Commun 47:10245–10247
33. Sabbah EN, Kadouche J, Ellison D et al (2007) In vitro and in vivo comparison of DTPA- and DOTA-conjugated antiferritin monoclonal antibody for imaging and therapy of pancreatic cancer. Nucl Med Biol 34:293–304
34. Runge VM, Jacobson S, Wood ML et al (1988) MR imaging of rat brain glioma: Gd-DTPA versus Gd-DOTA. Radiology 166:835–838
35. Thakur ML, Zhang K, Paudyal B et al (2011) Targeting apoptosis for optical imaging of infection. Mol Imaging Biol 14:163–171
36. Aziz RK, Kansal R, Aronow BJ et al (2010) Microevolution of group A streptococci in vivo: capturing regulatory networks engaged in sociomicrobiology, niche adaptation, and hypervirulence. PLoS One 5:e9798
37. Konig C, Simmen HP, Blaser J (1998) Bacterial concentrations in pus and infected peritoneal fluid—implications for bactericidal activity of antibiotics. J Antimicrob Chemother 42:227–232
38. van Oosten M, Schafer T, Gazendam JAC et al (2013) Real-time in vivo imaging of invasive- and biomaterial-associated bacterial infections using fluorescently labelled vancomycin. Nat Comm 4:3584
39. Xiao S, Abu-Esba L, Turkyilmaz S et al (2013) Multivalent dendritic molecules as broad spectrum bacteria agglutination agents. Theranostics 3:658–666
40. Ocakoglu K, Bayrak E, Onursal M et al (2011) Evaluation of Tc-99m-pheophorbide-a use in infection imaging: a rat model. Appl Radiat Isot 69:1165–1168
41. Akhtar MS, Iqbal J, Khan MA et al (2004) 99mTc-labeled antimicrobial peptide ubiquicidin (29–41) accumulates less in *Escherichia coli* infection than in *Staphylococcus aureus* infection. J Nucl Med 45:849–856
42. Ferro-Flores G, de Murphy CA, Pedraza-Lopez M et al (2003) In vitro and in vivo assessment of Tc-99m-UBI specificity for bacteria. Nucl Med Biol 30:597–603
43. Welling MM, Mongera S, Lupetti A et al (2002) Radiochemical and biological characteristics of Tc-99m-UBI 29-41 for imaging of bacterial infections. Nucl Med Biol 29:413–422
44. Roohi S, Mushtaq A, Malik SA (2005) Synthesis and biodistribution of Tc-99m-vancomycin in a model of bacterial infection. Radiochim Acta 93:415–418
45. Hertlein T, Sturm V, Kircher S et al (2011) Visualization of abscess formation in a murine thigh infection model of

staphylococcus aureus by F-19-magnetic resonance imaging (MRI). PLoS One 6:e18246
46. Kaim AH, Wischer T, O'Reilly T et al (2002) MR imaging with ultrasmall superparamagnetic iron oxide particles in experimental soft-tissue infections in rats. Radiology 225:808–814
47. Kaim AH, Jundt G, Wischer T et al (2003) Functional-morphologic MR imaging with ultrasmall superparamagnetic particles of iron oxide in acute and chronic soft-tissue infection: Study in rats. Radiology 227:169–174
48. Hnatowich DJ, Rusckowski M, Brill AB et al (1990) Pharmacokinetics in patients of an anti-carcinoembryonic antigen antibody radiolabeled with In-111 using a novel diethylenetriamine pentaacetic acid chelator. Cancer Res 50:7272–7278
49. Jenne CN, Kubes P (2013) Immune surveillance by the liver. Nat Immunol 14:996–1006
50. Gao B, Jeong WI, Tian ZG (2008) Liver: an organ with predominant innate immunity. Hepatology 47:729–736